Moisture Dependent Diffusion and Shrinkage in Yam during Drying

Amankwah, E. A., Dzisi, K. A., van Straten, G., & van Boxtel, A. J. B.

Increased water-use efficiency and reduced CO_2 uptake by plants during droughts at a continental-scale

Wouter Peters*[1,2], Ivar R. van der Velde[3,4], Erik van Schaik[1], John B. Miller[4], Philippe Ciais[5], Henrique F. Duarte[6], Ingrid T. van der Laan-Luijkx[1], Michiel K. van der Molen[1], Marko Scholze[7], Kevin Schaefer[8], Pier Luigi Vidale[9], Anne Verhoef[10], David Wårlind[7], Dan Zhu[5], Pieter P. Tans[4], Bruce Vaughn[11], James W.C. White[11]

CORRESPONDING AUTHOR

Correspondence on this manuscript and requests for data and material should be addressed to Wouter Peters (Wouter.Peters@wur.nl).

AUTHOR AFFILIATIONS

1. Environmental Sciences Group, Wageningen University, Wageningen, The Netherlands
2. University of Groningen, Centre for Isotope Research, Groningen, The Netherlands
3. Cooperative Institute for Research in Environmental Sciences, University of Colorado, Boulder, CO, United States
4. Global Monitoring Division, NOAA Earth System Research Laboratory, Boulder, CO, United States
5. Laboratoire des Sciences du Climat et de l'Environnement, LSCE/IPSL, CEA-CNRS-UVSQ, Gif sur Yvette, France
6. Dept. of Atm. Sciences, University of Utah, Salt Lake City, Utah, United States
7. Dept. of Physical Geography and Ecosystem Science, Lund University, Lund, Sweden
8. National Snow and Ice Data Center, University of Colorado, Boulder, CO, United States
9. Dept. of Meteorology, University of Reading, Reading, UK
10. Dept. of Geography and Environmental Science, University of Reading, Reading, UK
11. Institute for Arctic and Alpine Research, University of Colorado, Boulder, CO, United States

MAIN TEXT

Severe droughts in the Northern Hemisphere cause widespread decline of agricultural yield, reduction of forest carbon uptake, and increased CO_2 growth rates in the atmosphere. Plants respond to droughts by partially closing their stomata to limit their evaporative water loss, at the expense of carbon uptake by photosynthesis. This trade-off maximizes their water-use efficiency, as measured for many individual plants under laboratory conditions and field experiments. Here we analyze the $^{13}C/^{12}C$ stable isotope ratio in atmospheric CO_2 (reported as $\delta^{13}C$) to provide new observational evidence of the impact of droughts on the water-use efficiency across areas of millions of km^2 and spanning one decade of recent climate variability. We find strong and spatially coherent increases in water-use efficiency along with widespread reductions of net carbon uptake over the Northern Hemisphere during severe droughts that affected Europe, Russia, and the United States in 2001-2011. The impact of those droughts on water-use efficiency and carbon uptake by vegetation is substantially larger than simulated by the land-surface schemes of six state-of-the-art climate models. This suggests that drought induced carbon-climate feedbacks may be too small in these models and improvements to their vegetation dynamics using stable isotope observations can help to improve their drought response.

Global cycles of carbon and water are linked through plant stomata that open and close in response to levels of atmospheric CO_2 and humidity surrounding the leaf, as well as to soil moisture availability at the plants' roots[1,2,3,4]. By actively regulating the stomatal aperture, plants have been able to photosynthesize at a lower stomatal conductance and thus lower transpiration rate as a result of the atmospheric CO_2 increase of the past decades[5,6,7,8,9], leading to increased water-use efficiency at the leaf level (WUE, the gain of carbon per unit of water lost[10]). On top of this long-term response to CO_2, varying degrees of plant stress due to droughts cause year-to-year variations in water-use efficiency as frequently recorded in direct measurements of carbon and water fluxes at the ecosystem level[11,12]. Ecosystem-wide reductions in CO_2 exchange can in turn affect the annual global atmospheric CO_2 growth rate, if a drought is large and severe enough in extent[13,14]. At this spatiotemporal scale droughts, amongst other factors, influence the climate-carbon feedback on atmospheric CO_2. This is a poorly constrained property of contemporary

climate models and largely responsible for a strong divergence in their simulated atmospheric CO_2 levels and temperatures at the end of the 21st century[15,16].

WATER-USE EFFICIENCY AND CARBON ISOTOPES

The ratio of $^{13}C/^{12}C$, often denoted as $\delta^{13}C$, in vegetation has historically provided important information on vegetation drought dynamics[7,9,17]. This is because at the leaf-level, transport of atmospheric CO_2 through the stomata to the chloroplast and its subsequent photosynthesis both favor the lighter $^{12}CO_2$ molecule over the heavier $^{13}CO_2$ molecule at several stages[18]. This leads to lower $\delta^{13}C$ values in vegetation relative to the atmosphere, the difference denoted by the symbol Δ (units of ‰) and called "fractionation" or "discrimination". We use the latter term from hereon and refer to the Methods for further definitions.

Importantly, both discrimination and water-use efficiency scale linearly with the ratio of leaf-internal and atmospheric CO_2 (C_i/C_a). Under drought stress, stomatal closure decreases conductance and lowers the C_i/C_a ratio, leading to reduced photosynthesis, a smaller discrimination and a higher intrinsic water-use efficiency (iWUE, see Eqs 1 & 2 of Methods). This closure of stomata is reflected in both the vegetation (δ_v), and atmospheric (δ_a) isotopic ratios following photosynthetic CO_2 uptake in leaves. However, an advantage of using δ_a rather than δ_v to study changes in water-use efficiency is that the atmosphere integrates signals of surface CO_2 exchange over large areas[19] because air masses are transported and mixed rapidly in the turbulent lower atmosphere.

Here, we present new evidence that widespread increases in iWUE of vegetation during severe droughts in the Northern Hemisphere were recorded in atmospheric records of the $\delta^{13}C$ of CO_2 in air ($\delta^{13}C_a$), sampled from the NOAA Global Greenhouse Gas Reference Network between 2001 and 2011. We analyzed the mole fractions of CO_2 and its $\delta^{13}C_a$ in more than 25,000 air samples collected on a weekly basis at 53 sites mostly located in the Northern Hemisphere (see Suppl. Inf. S2 for a map of sampling locations). Our method relies on a separately published data assimilation technique[20] to simultaneously interpret these measurements, yielding spatiotemporal patterns of Net Ecosystem Exchange (NEE, defined here as negative when CO_2 is taken up from the atmosphere) and Δ.

Our analysis reveals a high correlation and significant slope ($r=-0.86$, $p=0.001$) between interannual variations in NEE and Δ when integrated over the Northern Hemisphere land biosphere

(Fig 1). In years when annual mean NEE is low (less net carbon uptake, a positive NEE anomaly), Δ is low too (less discrimination, a negative Δ anomaly), implying that stomata have partially closed. This correlated response in the land biosphere is not found with a traditional NEE estimate based on atmospheric CO_2 observations alone, and neither is it found if δ_a observations are used as in previous studies to estimate terrestrial NEE but not discrimination (see Table 3 in [20] and Suppl. Info S4). Rather, this information is derived from the combined atmospheric CO_2 and $\delta^{13}C_a$ observations and provides a unique line of observational evidence on the land-atmosphere coupling of water and carbon at continental scales. Our analysis identifies extensive and severe mid-latitude droughts as the driver behind this correlation.

SEVERE DROUGHT IMPACTS

Four major droughts in our reanalysis (2002, 2003, 2006, and 2010) illustrate the low-NEE and low-Δ end of Fig 1. In each of these years we identified conditions of severe to extreme drought as characterized by a Standardized Precipitation and Evapotranspiration Index[21] (SPEI) below -1.0 that covered an area of more than 6 million km^2 (>10% of the Northern Hemisphere land), shown in Fig 2a-d. These droughts, each associated with strong heatwaves, are described in literature as the North American drought of 2002[22,23], the Eurasian droughts of summer 2003[13] and 2006[24], and the Russian drought of summer 2010[25,26]. Independent of SPEI, we derive changes in NEE and Δ over the Northern Hemisphere from our assimilation of atmospheric CO_2 and $\delta^{13}C_a$ (Fig 2e-h). Large areas of low SPEI cluster with areas of independently determined anomalous Δ and NEE, at least on scales of thousands of kilometers constrained by the 53-site global $\delta^{13}C$ network. The slope and correlations between NEE and Δ remain robust when integrating over temperate land regions (Europe + temperate North America + temperate Eurasia, $r=-0.79$, $p<0.05$), and over boreal land regions (boreal North America + boreal Eurasia, $r=-0.67$, $p<0.05$). Negative correlations with a smaller significance ($p<0.10$) persist in continental regions of Europe, boreal Eurasia, and boreal North America, but break down below that scale. Note that signals from tropical forests, although highly relevant for coupled carbon climate feedbacks, cannot be detected until we expand the monitoring efforts for $\delta^{13}C$ in CO_2 into these areas.

Integrated over the low-Δ areas in Fig 2e-h, the annual NEE anomalies amount to 270, 290, 360, and 130 TgC/yr of reduced carbon uptake for each of the respective years, which is close to 15% of the annual total net terrestrial uptake of the Northern Hemisphere (-2.5±0.46 PgC/yr[20]). Most of this anomaly is incurred during the NH summer months (Fig 2i-m) with the exception of 2006 where the summer drought anomaly was exacerbated by large net terrestrial carbon release in Europe

during the fall, likely due to the impact of record warm temperatures[27] on heterotrophic respiration. We note that fire emissions over the drought areas also increased by more than 2-σ of its 11-year interannual variability (IAV), but these anomalies still amount to only ~0.02 PgC/yr at these latitudes. Our results agree with independent reports of reductions in net carbon uptake for North America[23,28], Europe[29,30], and Russia[26,31] derived from eddy-covariance measurements, inverse models, remote-sensing data, and terrestrial biosphere models. Reductions in water-use efficiency in agree with independent measurements at a suite of eddy-covariance sites (Suppl. Info S5).

The area-averaged reductions in Northern Hemisphere Δ (mean=18.2‰) are 1.5-1.7‰ and exceed the standard deviation of the IAV over 11 years in their respective domains (shown in Fig 2e-h). Both relative humidity and soil moisture content are below their 1-σ deviation as well and we interpret these anomalies in Δ as reductions in C_i/C_a of the underlying C3 vegetation, resulting from drought stress at the leaves, and/or at the roots of the plants. Other factors can affect Δ-values as well, such as variable contributions in gross primary production (GPP) from C3 and C4 vegetation, variations in mesophyll conductance, and post-photosynthetic discrimination[32,33]. However, previous work[34] suggests that the contribution from these terms specifically to IAV in atmospheric $\delta^{13}C_a$ is likely to be small, and in the case of post-photosynthetic discrimination, not sufficiently understood to include on the scales considered here (also see Suppl. Info. S3).

A reduction of 1.5‰ in Δ during a large drought corresponds to a reduction in C_i/C_a ratio of ~0.06 (see Suppl. Fig S1), which is modest given a typical C_i/C_a ratio of ~0.7 in C3 vegetation with substantial variations (±0.1) in a single plant or ecosystem[35,36,37], as a function of variations in vapor pressure deficit (VPD). We consider the corresponding increase in iWUE of ~16 μmol/mol (see Suppl. Info S1) large though, especially in view of the very large surface area (>2 million km^2) and the considerable integration period of multiple summer months. Over such large space and time scales much of the local variability in VPD, C_i/C_a, and iWUE typically averages out because not all vegetation is under stress all the time and because neighboring ecosystems can show different responses to drought stress[10]. In contrast to such local variations, the area integrated response left a large and detectable impact on the atmosphere due to its spatial and temporal extent.

MODELED DROUGHT IMPACTS

The relationships between net carbon uptake and water-use efficiency we have derived from atmospheric CO_2 and $\delta^{13}C$ provide new targets to improve the coupling of carbon and water exchange at the land-surface in Earth System Models[6,38]. Here, we consider six terrestrial biosphere models used extensively in carbon cycle studies, and in climate simulations under CMIP5[39] and CMIP6[40]. Three of the models we assessed simulate full $\delta^{13}C$ cycling through

vegetation and soils, and attempt to simulate multiple sources of IAV in Δ (i.e., local changes in Δ, continental shifts in GPP from C3 and C4 dominated areas, variability in heterotrophic respiration). For the other models, we approximate simulated monthly Δ-values from their available C_i/C_a ratios using Eq (1), which captures >90% of the variations in Δ for C3-vegetation according to the fully isotope-enabled simulations (see Suppl. Info S1). This makes C_i/C_a ratios an excellent proxy to use in a $\delta^{13}C$-based analysis.

Fig 3 shows the model-simulated Δ-NEE relations for vegetated land areas compared to our new observational atmospheric constraint derived from $\delta^{13}C_a$ and CO_2. Only two models simulate a statistically significant negative relationship ($p<0.05$) between NEE and Δ across the NH, but with less than half the slope derived from atmospheric observations. Year-to-year changes in net carbon uptake and iWUE are typically weakly coupled in the models, with temporal correlation coefficients smaller than derived from atmospheric data, and a strong lack of interannual variability in Δ. The lack of strong NEE-Δ coupling is surprising, as each of these models has been parameterized such that C3 vegetation responds to droughts by closing stomata, reducing photosynthesis, and reducing transpiration, in agreement with ecosystem and laboratory measurements[10,29,41]. However, the new relationship we present here requires not just this response to be well-captured, but also the much less studied effect of droughts on C_i/C_a ratios, on NEE (consisting of both GPP and respirations from soils), and on their simultaneous variations. Our analysis shows large differences between the models in simulated land-atmosphere exchange when considering these variations. Currently, none of the models presented agree with the large-scale constraints imposed by the atmospheric CO_2 and $\delta^{13}C_a$.

We specifically calculated the simulated changes in NEE and Δ during the well-documented European extreme drought event of 2003 to illustrate its impact on carbon exchange. Relative to the inversely derived reduction of annual mean NEE (80 TgC/yr) and Δ (0.64‰, which translates to a 13% increase in iWUE in agreement with the 9-site average of 11.3% in Table S3), we see that the LPJ-GUESS model best matches the change in Δ but at a reduced rate of carbon uptake (623 TgC/yr) that is much larger than observed. This is because its respiration anomaly is much smaller than its GPP response in contrast to most other models, as there is no response of respiration to lower soil moisture (see Suppl. Info Table S4). In contrast, ORCHIDEE-MICT and JULES come closest to the reduction of net carbon uptake (79 TgC/yr, and 135 TgC/yr) but with a substantially underestimated reduction in Δ (0.21-0.29‰) and a large difference between each model's response in GPP and respiration (See Suppl. Info Fig S9). In a coupled-carbon-climate framework, this impact would also extend to the simulated hydrological cycle by further reductions

of transpiration, increases in atmospheric entrainment, and enhancement of the negative feedback on VPD in the atmosphere[42,43,44] during droughts.

MODELED DROUGHT RESPONSES

The spread between the models results from both the soil moisture and leaf-level water stress approaches they adopted. Their subsequent influence on carbon and water exchange is notoriously difficult to separate in ecosystem and laboratory observations[6,32,38,41,44]. Whereas drought stress induced by high VPD is dominant on scales of hours to weeks, soil moisture limitations additionally come into play at scales of weeks to seasons. Novick et al.[45] showed that in forested ecosystems, soil moisture stress contributed on average 40% to the total reduction in growing season surface conductance. During prolonged droughts, soil moisture drought stress limits biochemical functioning (e.g., carboxylation and electron transport rates; biochemical limitations), as well as conductance of the mesophyll, xylem, and stomata (stomatal limitations). Egea et al.[46] showed that in the coupled assimilation-conductance approach used in all these models, incorporation of both limitations simultaneously is needed to increase iWUE during droughts, and best reproduces a wide range of observations in different types of vegetation. At the leaf-level, the drought responses of all six models rely on well-established formulations of the coupled assimilation-conductance system that have been characterized and compared to observations extensively (see online Methods and Suppl. Info S6). On the other hand, the effect of soil-moisture stress on iWUE varies widely between the models. Most of them consider only biochemical limitations, or only stomatal limitations, or have used formulations which reduce GPP and g_s, but compensate to keep C_i/C_a, and hence iWUE, constant[46]. These models could thus agree in principle with atmospheric CO_2-based analysis of net carbon uptake, but do not yet match the combined $\delta^{13}C_a$ and CO_2 constraints from the atmosphere.

Within CMIP6, and specifically its coupled carbon climate model inter comparison (C4MIP), the use of isotopically derived constraints on model performance was specifically called for[40] as the treatment of coupled carbon-water exchange represents a major opportunity for model improvement[6,9,47,48,49]. Our use of multiple years of atmospheric $\delta^{13}C_a$ records in this reanalysis supports such model development, and highlights a need to better represent the interannual variations in the conductance of CO_2 by stomata and the mesophyll, and to consider possible biochemical limitations to carbon uptake during drought stress resulting from low soil moisture. Our work demonstrates that valuable and unique information can be derived from a global long-term

monitoring effort of $\delta^{13}C$ in atmospheric CO_2, to potentially improve our understanding of vegetation drought responses at the largest, and most climate-relevant, scales.

REFERENCES

1. Monteith, J. L. Evaporation and environment. *Proceedings of the Society for Experimental Biology* **19**, 205–234 (1965).
2. Jarvis, P. G. The Interpretation of the Variations in Leaf Water Potential and Stomatal Conductance Found in Canopies in the Field. *Phil. Trans. Roy. Soc. B* **273**, 593–610 (1976).
3. Teuling, A. J. et al. Contrasting response of European forest and grassland energy exchange to heatwaves. *Nat. Geosci.* **3**, 722–727 (2010).
4. Buckley, T. N. The Control of Stomata by Water Balance. *New Phytologist* **168**, 275–92, (2005)
5. Keenan, T. F. et al. Increase in forest water-use efficiency as atmospheric carbon dioxide concentrations rise. *Nature* **499**, 324–327 (2013).
6. Swann, A. L. S. et al. Plant Responses to Increasing CO_2 Reduce Estimates of Climate Impacts on Drought Severity. *Proc. Natl. Acad. Sci. USA* **113**, (2016).
7. van der Sleen, P. et al. No growth stimulation of tropical trees by 150 years of CO_2 fertilization but water-use efficiency increased. *Nat. Geosci.* **8**, 24–28 (2015).
8. Keeling, R. F. et al. Atmospheric Evidence for a Global Secular Increase in Carbon Isotopic Discrimination of Land Photosynthesis. *Proc. Natl. Acad. Sci. USA* 114 (2017).
9. Frank, D. C. et al. Water-Use Efficiency and Transpiration Across European Forests During the Anthropocene. *Nat. Clim. Change* **5,** 579–83 (2015).
10. Medlyn, B. et al. How Do Leaf and Ecosystem Measures of Water-Use Efficiency Compare? *New Phytologist* **216**, 758–70 (2017).
11. Reichstein, M. et al. Severe drought effects on ecosystem CO_2 and H_2O fluxes at three Mediterranean evergreen sites: revision of current hypotheses? *Glob. Change Biol.* **8**, 999–1017 (2002).
12. Bowling, D. et al. Partitioning net ecosystem carbon exchange with isotopic fluxes of CO_2. *Glob. Change Biol.* **7**, 127–145 (2001).
13. Ciais, P. et al. Europe-wide reduction in primary productivity caused by the heat and drought in 2003. *Nature* **437**, 529–533 (2005).
14. Jung, M. et al., Compensatory Water Effects Link Yearly Global Land CO_2 Sink Changes to Temperature. *Nature* **541**, 516–20 (2017).
15. Booth, B. B. et al. High sensitivity of future global warming to land carbon cycle processes. *Env. Res. Let.* **7**, 024002-8 (2012).

16. Piao, S. et al. Evaluation of terrestrial carbon cycle models for their response to climate variability and to CO_2 trends. *Glob. Change Biol.* **19**, 2117–2132 (2013).

17. Köhler, I. H. et al. Intrinsic water-use efficiency of temperate semi-natural grassland has increased since 1857: an analysis of carbon isotope discrimination of herbage from the Park Grass Experiment. *Glob. Change Biol.* **16**, 1531– 1541 (2010).

18. Farquhar, G. D. et al. On the Relationship Between Carbon Isotope Discrimination and the Intercellular Carbon Dioxide Concentration in Leaves, *Aust. J. Plant Physiol.* **9**, 121 – 137 (1982).

19. Ballantyne, A. P. et al., Apparent seasonal cycle in isotopic discrimination of carbon in the atmosphere and biosphere due to vapor pressure deficit. *Glob. Biogeochem. Cyc.* **24**, GB3018 (2010).

20. van der Velde, I.R. et al. The CarbonTracker Data Assimilation System for CO_2 and $\delta^{13}C$ (CTDAS-C13 v1.0): Retrieving Information on Land–Atmosphere Exchange Processes." *Geosci. Model Dev.* **11**, 283–304 (2018)

21. Vicente-Serrano, S. M. et al. A Multiscalar Drought Index Sensitive to Global Warming: The Standardized Precipitation Evapotranspiration Index. *J. Clim* **23**, 1696-1718 (2010).

22. Mekonnen, Z.A. et al. Carbon Sources and Sinks of North America as Affected by Major Drought Events During the Past 30 Years. *Agr. Forest Meteorol.* **244-245**, 42-56 (2017).

23. Schwalm, C. R. et al. Reduction in carbon uptake during turn of the century drought in western North America. *Nat. Geosci.* 5, 551–556 (2012).

24. Spinoni, J. et al. The biggest drought events in Europe from 1950 to 2012. *J. Hydr Regional Studies* **3**, 509-524 (2015).

25. Yurganov, L. N. et al. Satellite- and ground-based CO total column observations over 2010 Russian fires: accuracy of top-down estimates based on thermal IR satellite data. *Atm. Chem. Phys.* **11**, 7925–7942 (2011).

26. Krol, M. et al. How much CO was emitted by the 2010 fires around Moscow? *Atm. Chem. Phys.* **13**, 4737–4747 (2013).

27. Luterbacher, J. et al. Exceptional European warmth of autumn 2006 and winter 2007: Historical context, the underlying dynamics, and its phenological impacts. *Geoph. Res. Let.* **34**, L12704 (2007).

28. Peters, W. et al. An atmospheric perspective on North American carbon dioxide exchange: CarbonTracker. *Proc. Natl. Acad. Sci. USA* **104**, 18925–18930 (2007).

29. Reichstein, M. et al. Reduction of ecosystem productivity and respiration during the European summer 2003 climate anomaly: a joint flux tower, remote sensing and modelling analysis. *Glob. Change Biol*. **13**, 634–651 (2007).

30. Peters, W. et al. Seven years of recent European net terrestrial carbon dioxide exchange constrained by atmospheric observations. *Glob. Change Biol.* **16**, 1317–1337 (2010).

31. Guerlet, S. et al. Reduced carbon uptake during the 2010 Northern Hemisphere summer from GOSAT. *Geoph. Res. Let.* **40**, 2378–2383 (2013).

32. Werner, C. et al. Linking Carbon and Water Cycles Using Stable Isotopes Across Scales: Progress and Challenges. *Biogeosci*. **9**, 3083-3111 (2011).

33. Brüggemann, N. et al. Carbon allocation and carbon isotope fluxes in the plant-soil-atmosphere continuum: a review. *Biogeosci*. **8**, 3457-3489 (2011).

34. van der Velde, I. R. et al., Biosphere model simulations of interannual variability in terrestrial 13C/12C exchange, *Glob. Biogeochem. Cyc.* **27**, 637–649 (2013).

35. Farquhar, G. Models of integrated photosynthesis of cells and leaves. *Phil. Trans. Roy. Soc. B* **323**, 357–367 (1989).

36. Baldocchi, D. An analytical solution for coupled leaf photosynthesis and stomatal conductance models. *Tree Physiology* **14**, 1069–1079 (1994).

37. Beer, C. et al. Temporal and Among-Site Variability of Inherent Water Use Efficiency at the Ecosystem Level. *Glob. Biogeochem. Cyc.* **23**, GB2018 (2009).

38. Mystakidis, S. et al. Hydrological and Biogeochemical Constraints on Terrestrial Carbon Cycle Feedbacks. *Env. Res. Let.* **12**, 014009-20 (2017).

39. Taylor, K. E. et al. An Overview of CMIP5 and the Experiment Design. *Bul. Am. Meteo. Soc.* **93**, 485–498. (2012).

40. Jones, C. D. et al. C4MIP - the Coupled Climate–Carbon Cycle Model Intercomparison Project: Experimental Protocol for CMIP6. *Geosci. Model Dev.* **9**, 2853–80 (2016).

41. Bodin, P. E. et al. Comparing the performance of different stomatal conductance models using modelled and measured plant carbon isotope ratios ($\delta^{13}C$): implications for assessing physiological forcing. *Glob. Change Biol.* **19**, 1709–1719 (2013).

42. Miralles, D. et al. Mega-Heatwave Temperatures Due to Combined Soil Desiccation and Atmospheric Heat Accumulation. *Nat. Geosci.* **7**, 345–49 (2014).

43. De Kauwe, M. G. et al. Ideas and Perspectives: How Coupled Is the Vegetation to the Boundary Layer? *Biogeosci*. **14**, 4435–53 (2017).

44. Zhou, S. et al. How Should We Model Plant Responses to Drought? an Analysis of Stomatal and Non-Stomatal Responses to Water Stress. *Agr. Forest Meteorol*. **182-183**, 204–14 (2013).

45. Novick, K. A. et al. The Increasing Importance of Atmospheric Demand for Ecosystem Water and Carbon Fluxes. *Nat. Clim. Change* **6**, 1023–27 (2016).

46. Egea, G. et al. Towards an Improved and More Flexible Representation of Water Stress in Coupled Photosynthesis-Stomatal Conductance Models. *Agr. Forest Meteorol*. **151**, 1370–84 (2011) .

47. Green, J. K. et al. Regionally Strong Feedbacks Between the Atmosphere and Terrestrial Biosphere. *Nat. Geosci.* **10**, 410–14 (2017).

48. Wang, H. et al. Towards a Universal Model for Carbon Dioxide Uptake by Plants. *Nat. Plants* **3**, 734–41 (2017).

49. Ukkola, A. M. et al. Land Surface Models Systematically Overestimate the Intensity, Duration and Magnitude of Seasonal-Scale Evaporative Droughts. *Env. Res. Let.* **11**, 104012-23 (2016).

ACKNOWLEDGEMENTS

This work used eddy covariance data acquired by the FLUXNET community. We acknowledge the financial support to the eddy covariance data harmonization provided by CarboEuropeIP, FAO-GTOS-TCO, iLEAPS, Max Planck Institute for Biogeochemistry, National Science Foundation, University of Tuscia, Université Laval and Environment Canada and US Department of Energy and the database development and technical support from Berkeley Water Center, Lawrence Berkeley National Laboratory, Microsoft Research eScience, Oak Ridge National Laboratory, University of California-Berkeley, University of Virginia. Ru-Fyo data was kindly provided by Andrej Varlagin and Julia Kurbatova from the Russian Academy of Sciences. Carsten Montzka is acknowledged for providing a SoilGrids-ROSETTA based set of soil-hydraulic properties for the JULES modeling effort. We thank John C. Lin and Brett M. Raczka for their contributions to the CLM4.5 work. We thank Sylvia E. Michel (INSTAAR) for QA/QC of the $\delta^{13}C$ data used in this study. Christian Rödenbeck is kindly acknowledged for providing additional information on gross ocean exchange. Ivar van der Velde was financially supported by the Netherlands Organization for Scientific Research (NWO-VIDI: 864.08.012) and by the National Computing Facilities Foundation (NCF project SH-060) for the use of supercomputing facilities. HFD was supported by the US Department of Energy's Office of Science, Terrestrial Ecosystem Science Program (award #DE-SC0010624), and by the NASA CMS Project (award #NNX16AP33G). Wouter Peters and Erik van Schaik received financial support from the European Research Council's project ASICA (CoG 649087). We thank the NOAA Climate Program Office's Atmospheric Chemistry, Carbon Cycle, and Climate (AC4) program for support, including that for collection and analysis of CO_2 and $\delta^{13}C$ observations used in this study. We thank three anonymous reviewers and Peter R. Rayner for very helpful comments on the manuscript.

AUTHOR CONTRIBUTIONS

W.P, I.vdV, and J.B.M designed the study. I.vdV, K.S, W.P., E.v.S., I.vd.L.L, P.L.V., A.V., P.C., D.W., M.S, D.Z., H.F.D, and M.vdM built the inverse and forward modeling frameworks. P.P.T, B.V., and J.W.C.W. were responsible for the $\delta^{13}C$ and CO_2 measurement program. W.P., I.vdV, and E.v.S. performed the analysis and wrote the main text. All authors gave input on the final manuscript.

COMPETING FINANCIAL INTERESTS

The authors declare no competing financial interests.

FIGURE CAPTIONS

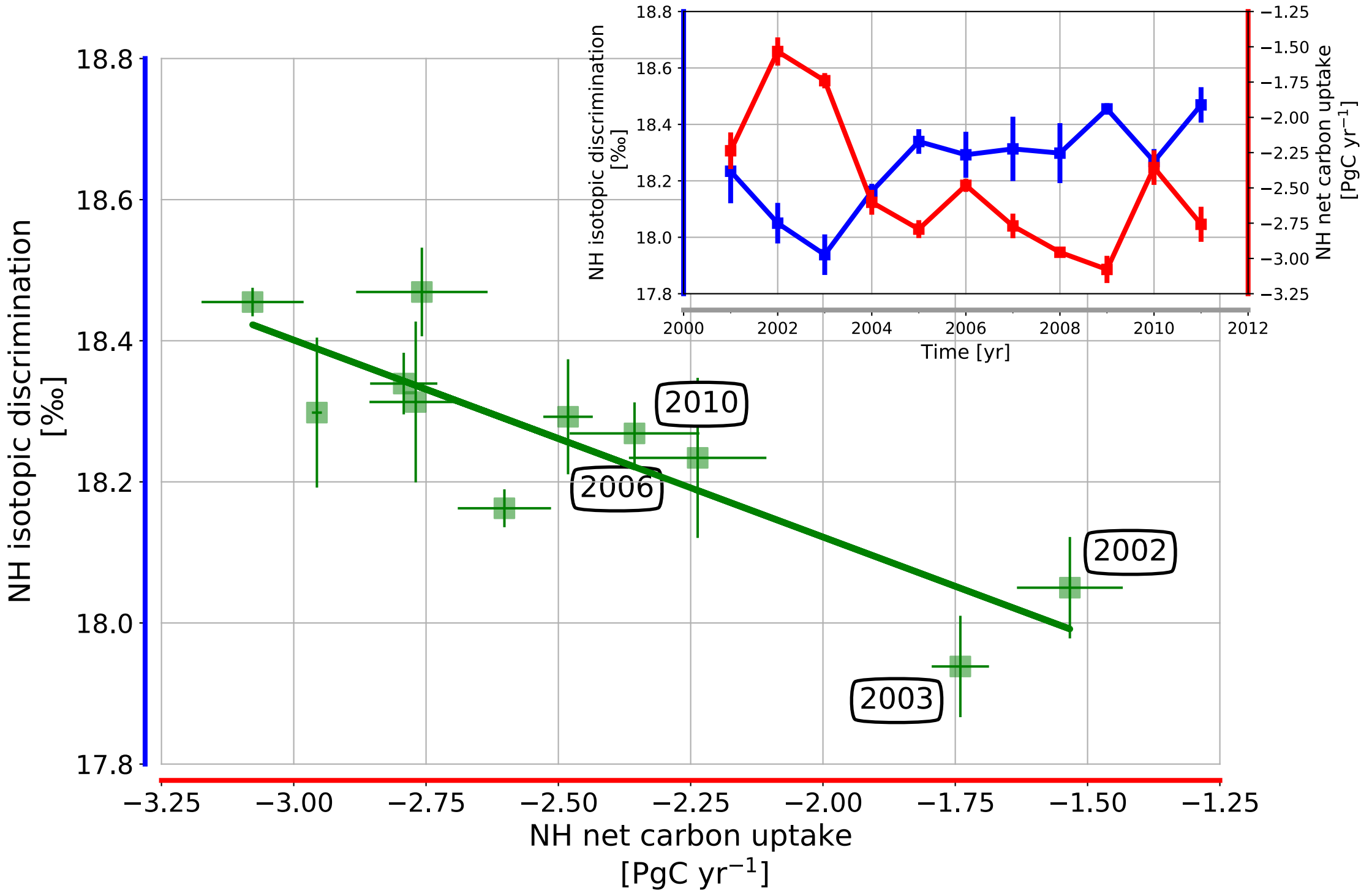
NH isotopic discrimination [‰]
NH net carbon uptake [PgC yr^{-1}]
2010
2006
2002
2003
Time [yr]

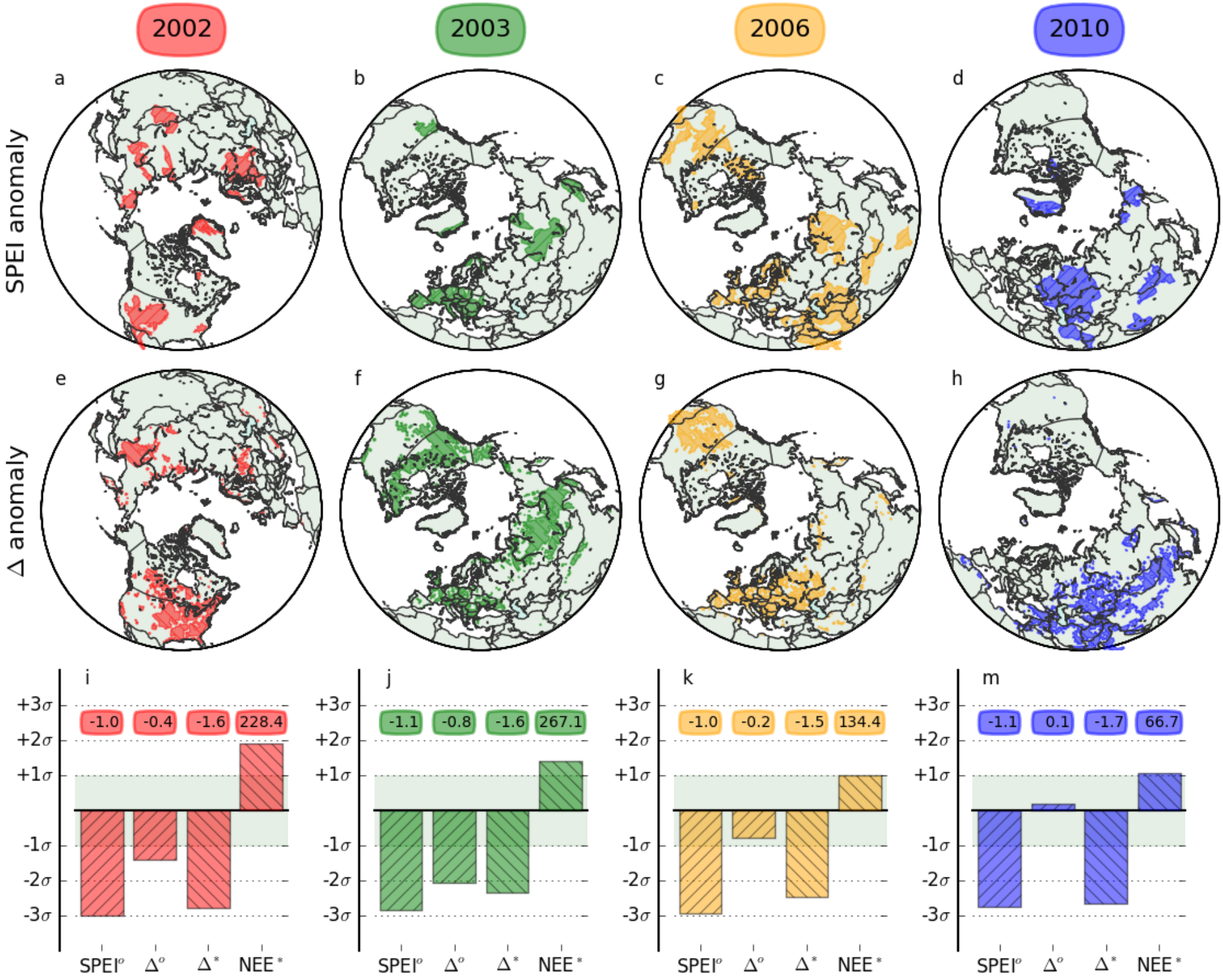
2002
2003
2006
2010
SPEI anomaly
Δ anomaly
a
b
c
d
e
f
g
h
i
j
k
m
+3σ
+2σ
+1σ
-1σ
-2σ
-3σ
-1.0
-0.4
-1.6
228.4
-1.1
-0.8
-1.6
267.1
-1.0
-0.2
-1.5
134.4
-1.1
0.1
-1.7
66.7
SPEI°
Δ°
Δ*
NEE*

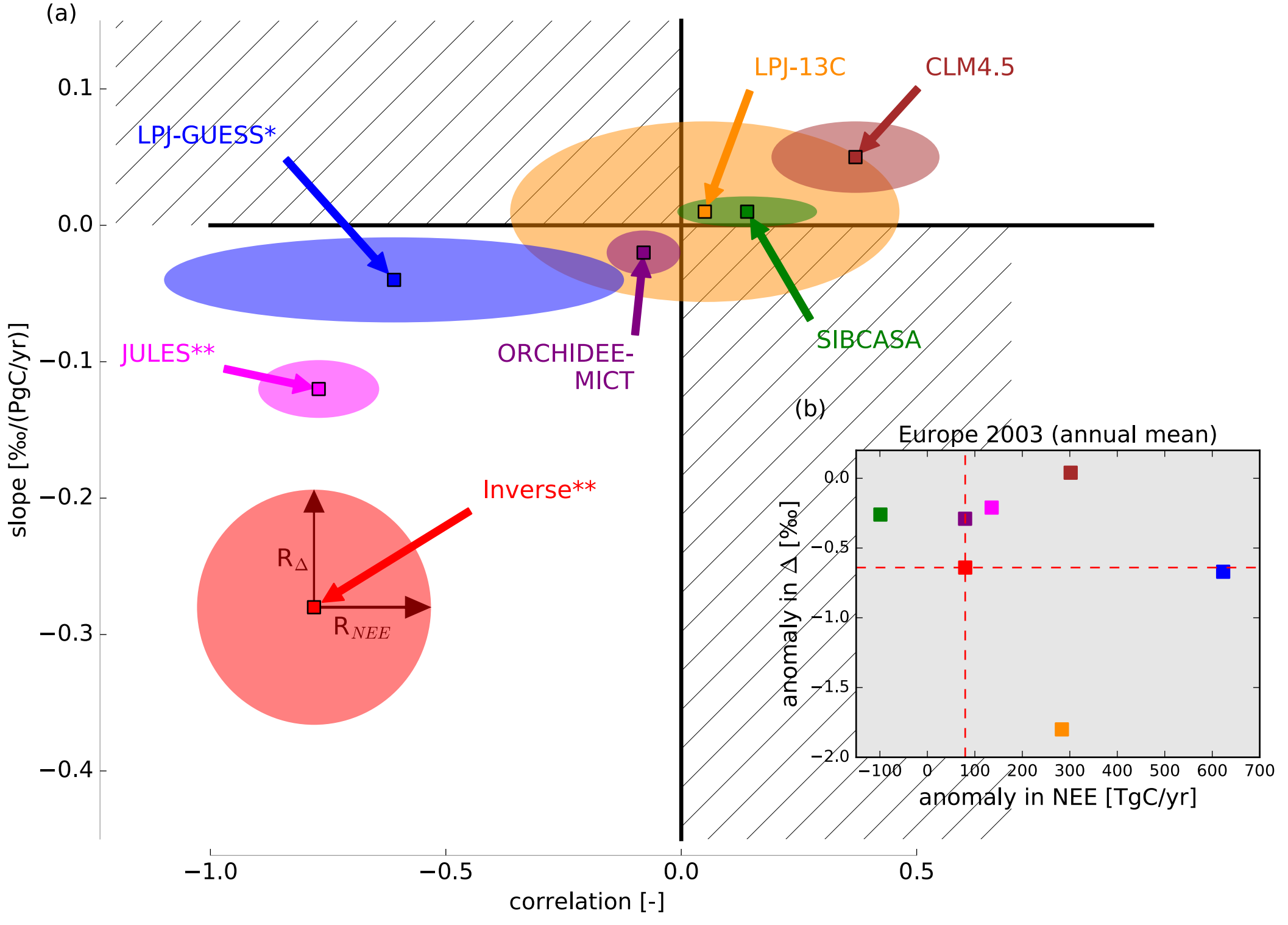
(a)
LPJ-13C
CLM4.5
LPJ-GUESS*
JULES**
ORCHIDEE-
MICT
SIBCASA
Inverse**
R_Δ
R_{NEE}
slope [‰/(PgC/yr)]
correlation [-]
0.1
0.0
−0.1
−0.2
−0.3
−0.4
−1.0
−0.5
0.0
0.5
(b)
Europe 2003 (annual mean)
anomaly in Δ [‰]
anomaly in NEE [TgC/yr]
0.0
−0.5
−1.0
−1.5
−2.0
−100
0
100
200
300
400
500
600
700

Figure 1: Annual mean net carbon uptake (NEE, defined as negative when CO_2 is taken up by the biosphere) versus isotopic discrimination integrated over Northern Hemisphere land area. The slope of the green regression line is -0.28±0.13 ‰/PgCyr^{-1}. Error bars show 1-σ standard deviations based on four alternative approaches to the data assimilation estimates (see Table S2 of the Suppl. Info). Inset shows the temporal correlation between the two time-series (r=-0.86), partly explained by a secular trend in both variables, but mostly by correlated interannual variations (r=-0.74, see Methods).

Figure 2: Severe droughts in the period 2001-2011 as recorded independently in the SPEI index (< -1.0, top row) and in the estimated discrimination of vegetation against $^{13}CO_2$ (Δ anomalies, middle row). Colored areas experienced anomalies >1-σ relative to the 11-year mean. Shown are the summer (JJA) droughts in (a and e) North America 2002, (b and f) Europe 2003, (c and g) Europe 2006, and (d and h) Russia 2010. (i-m) shows the JJA integrated anomalies in SPEI index, Δ, and NEE divided by their standard deviation. Symbols (o) or (*) denote integration over the contours shown in the top (a-d) or middle row (e-h) respectively. Labels show the absolute anomalies in units of [-], [‰], [‰], and [TgC/yr].

Figure 3: The statistics of the NH NEE-Δ relationship from 2001-2011 derived from atmospheric data (red) and from six global vegetation models. In (a), colored squares represent the values for the estimated correlation (x-axis) and slope (y-axis) of the relationship. Slopes significantly different from 0.0 are denoted as ** p<0.001, * p<0.05 for N=9, two-sided t-test. The red circle illustrates one standard deviation of the IAV in NEE and in Δ (R_{NEE} = 0.49 PgC/yr, R_{Δ} = 0.18 ‰) around the inverse estimate. IAV of each model can be quantitatively assessed from the radii of its ellipse relative to this red circle. (b) shows the annual mean anomaly in Δ (x-axis) and NEE (y-axis) for the 2003 drought in Europe for the same set of models and observations. Positive NEE anomalies signify reduced carbon uptake during droughts, while negative anomalies in Δ signify increased iWUE.

METHODS

The analysis presented uses measurements of CO_2 and $\delta^{13}C_a$ in air from flasks collected as part of the Global Greenhouse Gas Reference Network at the NOAA Earth System Research Laboratory and analyzed at NOAA for CO_2 and at the University of Colorado Institute for Arctic and Alpine Research in Boulder, USA for $\delta^{13}C$. One standard deviation of CO_2 mole fraction differences reported for flask pairs is 0.1 to 0.25 ppm, depending on the site, while measured $\delta^{13}C_a$ ratio differences between sample pairs is 0.02‰ to 0.03‰. All measurements have been carefully calibrated against the international scale for CO_2 (WMO CO_2 X2007) and the Vienna-PeeDee Belemnite scale for $\delta^{13}C_a$ over the full period we report on here. Whole air isotopic standards are additionally calibrated to Jena Reference Air Set (JRAS), a multi-point scale anchor for isotope measurements of CO_2 in air[50].

The relationship between intrinsic water-use efficiency (iWUE) and isotopic discrimination is widely used, following Farquhar[17] and Seibt[51] we can write:

$$\mathrm{iWUE} = \frac{A_n}{g_{s,h_2o}} \approx \frac{g_{s,co_2}(C_i - C_a)}{g_{s,h_2o}} \approx \frac{C_a(1 - C_i/C_a)}{1.6} \qquad (1)$$

$$\delta_a - \delta_v \approx \Delta \approx \Delta_d + (\Delta_p - \Delta_d)\frac{C_i}{C_a} \qquad (2)$$

iWUE relates the diffusion of water and CO_2 through stomata at a given C_a. A_n is the net carbon assimilation rate and Δ_p (27‰) and Δ_d (4.4‰) are the isotopic discriminations during assimilation catalyzed by the enzyme Rubisco in C_3 photosynthesis and molecular diffusion of CO_2 through the stomata, respectively. The ratio of molecular diffusion of H_2O to CO_2 is the factor 1.6 in Eq 1. Note that Eq (2) is a simplification of isotopic fractionation described in [17], focused on terms that drive the interannual variations of $\delta^{13}C$ in CO_2 rather than the decadal and longer-term changes[8].

The measurements are assimilated into a new framework for joint CO_2-$\delta^{13}C_a$ data assimilation presented separately in [20]. Briefly, it uses both atmospheric CO_2 and $\delta^{13}C_a$ observations (N=99,300) to simultaneously estimate biospheric NEE, biospheric Δ, and oceanic net carbon fluxes; fossil fuel and biomass burning emissions are fixed. An important innovation compared to previous studies[52,53] using similar δ_a records is that our system not only partitions net carbon uptake

between land (Net Ecosystem Exchange, or NEE, defined as negative when CO_2 is taken up from the atmosphere) and ocean, but it additionally uses these observations to optimize the isotopic discrimination associated with NEE (also see Suppl Info S3). Variations in $\delta^{13}C_a$ are thus interpreted as a proxy for changes in iWUE of vegetation across continental scales. The data assimilation system adjusted 460 parameters globally each week, where each parameter is associated with either the net CO_2 flux (NEE in mol/m^2/s) or discrimination value (Δ in ‰) of a large "ecoregion" or an oceanic net flux in one of 31 ocean basins (e.g. [28]). Each ecoregion corresponds to a plant-functional type from the Olson database within each continent. The optimized parameters combined with the a-priori NEE and Δ constitute an 11-year reanalysis of surface fluxes and discrimination used in Figs 1 and 2. In [20] and in the Suppl. Info, we included investigations of the robustness, linearity, and signal-to-noise of our results across the mentioned set of six inversions. These confirm that (a) the shown relationship only emerges when NEE and Δ are estimated simultaneously, and only when using both $\delta^{13}C_a$ and CO_2 as atmospheric constraints, (b) the NEE and Δ estimates do not covary in the posterior covariance matrix and are estimated independently, and (c) the non-linearity in the system of equations (NEE and Δ are multiplicative terms in the $\delta^{13}C_a$ budget) does not drive the relation: it can be linearized by first constraining NEE-only with $\delta^{13}C_a$ and CO_2, and then propagating the resulting ensemble of NEE to a Δ-only inversion. Error bars in Fig 1 (1-σ) are derived from the mentioned set of six.

All slopes of the curve fits in Fig 1 and Fig 3 were tested for differences from zero using two-tailed t-tests and a 95% confidence level for 9 degrees of freedom (nyears-2). Model-II (RMA) regression was used in determining the slopes of NEE vs Δ, and these were not different from using a simpler model-I (OLS) regression. In the main text, the significance of the slopes (p-value) is quoted along with the correlation coefficients (r), as derived from the Δ and NEE estimates over the full 11 year period, including the derived trend. The secular trend in Δ and NEE thus drives part of this correlation, and the correlation coefficient based on detrended time series (i.e., testing only the correlations in IAV) is slightly smaller (r=-0.74) than the full one (r=-0.86).

For analysis of the drought impacts we integrated signals to larger areas based on the selection of grid boxes north of 25 degrees latitude with anomalously low SPEI values (6-month time scale, >1σ negative anomaly relative to the 11-year IAV, shown in Figs 2a-d for contiguous areas >0.1 million km^2), or alternatively low Δ-values (>1σ negative anomaly relative to the 11-year IAV, shown

in Figs 2e-h). Spatial and temporal aggregation to the summer season (JJA) used the GPP and area of each grid box to weight its contribution to the total signal.

Models used in the analysis of Fig 3 and their calculated iWUE are documented in the Suppl. Info S6. For their analysis, monthly mean GPP-weighted C_i/C_a or Δ values from their output were used. To isolate the Northern Hemisphere land areas we used a mask from TRANSCOM (regions 1,2,7,8,11, see http://transcom.project.asu.edu/transcom03_protocol_basisMap.php). This mask was also applied to the inverse results in Fig 1, and to the inverse simulation B1 (see Suppl. Info S4) displayed in Fig 3. Analysis for Europe 2003 anomalies focused on a smaller area illustrated in the Suppl. Info Fig S10 and S11. A summary of drought response formulations in each model is provided in Suppl Info Table S4.

AVAILABILITY OF DATA

Observational data used in this study are available from NOAA ESRL and INSTAAR at https://www.esrl.noaa.gov/gmd/dv/data/. We specifically used Observation Package (ObsPack) version 1.0.3 for CO_2 and version 0.9.0 for isotope ratios of $^{13}C/^{12}C$. Model results used in the analyses are available from the permanent data repository at the ICOS Carbon Portal[54], under DOI 10.18160/0ZZK-FNK1

AVAILABILITY OF CODE

The CTDAS-C13 and TM5 source code are available at ftp://ftp.cmdl.noaa.gov/user/ivar/CTDAS_C13_sourcecode. Python Notebooks with the analysis of all results and resulting in the figures in the main text are available upon request.

METHODS REFERENCES

50. Wendeberg, M. et al. Jena Reference Air Set (JRAS): a multi-point scale anchor for isotope measurements of CO_2 in air. *Atm. Meas. Tech*. **6**, 817–822 (2013).

51. Seibt, U. et al. Carbon isotopes and water use efficiency: sense and sensitivity. *Oecologia* **155**, 441-454 (2008).

52. Ciais, P. et al. Partitioning of ocean and land uptake of CO_2 as inferred by $\delta^{13}C$ measurements from the NOAA Climate Monitoring and Diagnostics Laboratory Global Air Sampling Network. *J. Geoph. Res.* **100**, 5051–5070 (1995).

53. Rayner, P. J. et al. Interannual variability of the global carbon cycle (1992-2005) inferred by inversion of atmospheric CO_2 and $\delta(CO_2)$-C13 measurements. *Glob. Biogeochem. Cyc*. **22**, GB3008 (2008).

54. Peters et al. Carbon Portal dataset. https://doi.org/10.18160/0ZZK-FNK1 (2018)